

Multiple Ising Spins Coupled to 2d Quantum Gravity

M. G. HARRIS and J. F. WHEATER

Department of Physics
Theoretical Physics, University of Oxford,
1 Keble Road, Oxford OX1 3NP, UK
E-mail addresses: harris@thphys.ox.ac.uk and jfw@thphys.ox.ac.uk

Abstract

We study a model in which p independent Ising spins are coupled to 2d quantum gravity (in the form of dynamical planar ϕ^3 graphs). Consideration is given to the $p \rightarrow \infty$ limit in which the partition function becomes dominated by certain graphs; we identify most of these graphs. A truncated model is solved exactly providing information about the behaviour of the full model in the limit $\beta \rightarrow 0$. Finally, we derive a bound for the critical value of the coupling constant, β_c and examine the magnetization transition in the limit $p \rightarrow 0$.

1 Introduction

Models in which conformal matter of central charge c is coupled to 2d quantum gravity have attracted considerable interest. Much progress has been made for the case $c \leq 1$, using both continuum and discrete approaches. The former has yielded the KPZ formulae [1, 2, 3], which give as functions of the central charge the modification of critical exponents due to gravity. However, these formulae only apply for $c \leq 1$; for larger values of c they predict that the string susceptibility γ_{str} is complex, which does not make much sense. The discrete methods involve using dynamical triangulations coupled to matter fields. Matrix model techniques have proven to be extremely valuable for studying $c \leq 1$ models [4, 5, 6] and perturbative expansions allow one to investigate numerically the behaviour of γ_{str} for $c > 1$ [7, 8, 9]. The model in which a single Ising spin is attached to the face of each triangle has a central charge of one half and has been solved exactly [10, 11, 12, 13, 14], yielding results for the critical exponents that agree with those of the KPZ formulae. Recently some remarkable analytical progress has been made for the $c \rightarrow \infty$ limit by considering the low temperature expansion [15, 16, 17]. There is evidence that in this limit tree-like or branched polymer graphs dominate the behaviour of the model and this is supported by our results. Despite much effort no one has managed to solve analytically any other models for $c \geq 1$; however such models are well-defined and there is no obvious pathology at $c = 1$. Many Monte Carlo simulations have been performed [18, 19, 20, 21, 22, 23] in an attempt to investigate the behaviour near the $c = 1$ barrier and to discover whether the breakdown of KPZ theory is due to some change in the geometry, such as a transition to a branched polymer phase. So far these simulations have failed to produce any convincing evidence of such a phase transition at $c = 1$.

In this paper we study the properties of a model for which p independent Ising spins are attached

to the face of each triangle, giving a central charge of $c = p/2$. In section 2 we define precisely three slightly different models and in section 3 we examine the limit of large p , identifying most of the dominant graphs. A version of the model in which the free energy is truncated is used in section 4 to study the transition to behaviour typical of large p , in the limit of small β . In section 5 we study the properties of the magnetization transition, deriving a bound on the critical value of the coupling constant ($\beta_c \geq 0.549$) and looking at the nature of the transition in the limit $p \rightarrow 0$. In section 6 we conclude by discussing possible forms of the phase diagram and by relating our work to the results from various computer simulations and to analytical work carried out by other authors.

2 Definition of the model

The model is one of p independent Ising spins on each vertex of a random ϕ^3 graph (which is the dual graph of a triangulated random surface). For a fixed N -vertex ϕ^3 graph, G , with a single spin on each vertex, the Ising partition function is

$$Z_G = \frac{1}{Z_0} \sum_{\{S\}} \exp \left(\beta \sum_{\langle ij \rangle} S_i S_j \right), \quad (1)$$

with

$$Z_0 = 2^N (\cosh \beta)^{\frac{3N}{2}}, \quad (2)$$

where S_i is the spin on the i -th vertex of the graph, the sum over $\langle ij \rangle$ is a sum over nearest neighbours (by which we mean vertices that are connected by a line in the graph) and β is the coupling constant. The factor of Z_0^{-1} is introduced in order to simplify the formulae later on. We then sum over a set of ϕ^3 graphs, with N vertices and a fixed genus, g , to get the partition function,

$$Z_N(p) = \sum_G \frac{1}{s_G} (Z_G)^p. \quad (3)$$

Each graph is weighted by the symmetry factor s_G^{-1} , which is the reciprocal of the order of the symmetry group for that graph. The symmetry factors are inserted because they occur in the matrix model solution of the $p = 0$ and $p = 1$ cases. However, we could equally well take $s_G = 1$ in the above definition, giving us a slightly different model, which is nonetheless expected to have identical properties in the thermodynamic limit $N \rightarrow \infty$. Consequently we will often ignore the symmetry factors especially in the large N limit when we would expect the graphs not to be very symmetric and hence to have $s_G \approx 1$ anyway.

In this paper we work with planar diagrams (ie $g = 0$) and consider three different versions of this model, which differ with respect to the sets of graphs that are used. In model I, G runs over all the planar connected ϕ^3 graphs with N vertices. Model II is the same as model I, except that tadpoles are excluded so that the graphs are one-particle irreducible. For model III, tadpoles and self-energy terms are excluded giving two-particle irreducible graphs.

In the thermodynamic limit the partition function has the asymptotic form,

$$Z_N(p) = e^{\mu(p,\beta)N} N^{\gamma_{str}-3} \left(a_0 + \frac{a_1}{N} + \dots \right). \quad (4)$$

The free energy $\mu(p, \beta)$ is defined as

$$\mu(p, \beta) = \lim_{N \rightarrow \infty} \frac{1}{N} \log(Z_N(p)) \quad (5)$$

and discontinuities in its derivatives indicate the presence of a phase transition. Similarly, μ_G for a given graph, G , is defined by,

$$\mu_G(\beta) = \lim_{N \rightarrow \infty} \frac{1}{N} \log(Z_G). \quad (6)$$

The string exponent γ_{str} is believed to be universal and to depend only upon certain general characteristics of the model.

2.1 Matrix model results ($p = 0$ and $p = 1$)

The case $p = 0$, where there are no Ising spins, just corresponds to enumerating ϕ^3 graphs. The number of graphs $\mathcal{G}^{(1)}(N)$ in model I can be calculated, for example by matrix model methods [24] (see also [25, 26]) with the result,

$$\mathcal{G}^{(1)}(N) = \frac{8^{\frac{N}{2}} \Gamma(\frac{3N}{4})}{2(\frac{N}{2} + 2)! \Gamma(\frac{N}{4} + 1)} \underset{N \rightarrow \infty}{\sim} e^{\frac{1}{2} \log(12\sqrt{3})N} N^{-\frac{7}{2}}. \quad (7)$$

For models II and III, the number of N -vertex graphs are denoted by $\mathcal{G}^{(2)}(N)$ and $\mathcal{G}^{(3)}(N)$ respectively and can also be calculated giving,

$$\mathcal{G}^{(2)}(N) = \frac{2^{\frac{N}{2}} (\frac{3N}{2} - 1)!}{(\frac{N}{2})! (N + 2)!} \underset{N \rightarrow \infty}{\sim} e^{\frac{1}{2} \log(\frac{27}{2})N} N^{-\frac{7}{2}}, \quad (8)$$

$$\mathcal{G}^{(3)}(N) = \frac{(2N - 3)!}{(\frac{N}{2})! (\frac{3N}{2})!} \underset{N \rightarrow \infty}{\sim} e^{\frac{1}{2} \log(\frac{256}{27})N} N^{-\frac{7}{2}}. \quad (9)$$

It should be noted that all these models yield the asymptotic form given in (4) with $\gamma_{str} = -\frac{1}{2}$.

The $p = 1$ case has been solved analytically [10, 11] and has a third order phase transition from a disordered to a magnetized state. For model I, the critical value of the coupling constant is given by [13],

$$\beta_c = -\frac{1}{2} \log \left(\frac{1}{27} (2\sqrt{7} - 1) \right) \approx 0.9196, \quad (10)$$

and for model III [14],

$$\beta_c = \frac{1}{2} \log \left(\frac{108}{23} \right) \approx 0.7733. \quad (11)$$

In both cases, the critical exponents are $\alpha = -1$, $\beta = \frac{1}{2}$, $\gamma = 2$, $\delta = 5$, $\nu = \frac{3}{d_H}$ and $\eta = 2 - \frac{2d_H}{3}$, where d_H is some unknown dimension depending on the geometry of the graphs. Also, $\gamma_{str} = -\frac{1}{2}$ everywhere, except at the critical point, where $\gamma_{str}^* = -\frac{1}{3}$.

These results should be compared with those for a fixed regular lattice, such as the hexagonal lattice, for which,

$$\beta_c = \tanh^{-1} \left(\frac{1}{\sqrt{3}} \right) \approx 0.658 \quad (12)$$

and there is a second order magnetization transition with critical exponents: $\alpha = 0$, $\beta = \frac{1}{8}$, $\gamma = \frac{7}{4}$, $\delta = 15$, $\nu = 1$, $\eta = \frac{1}{4}$. Introducing the sum over triangulations changes the universality class, but the precise nature of the sum is not important.

3 Dominant graphs in the limit $p \rightarrow \infty$

3.1 Concavity of $\mu(p, \beta)$

In this section we will ignore the symmetry factors, however it is easy to show that all the results follow if we include them. Using the Cauchy-Schwartz inequality on (3) it follows that,

$$\left(Z_N \left(\frac{p+q}{2} \right) \right)^2 \leq Z_N(p) Z_N(q) \quad (13)$$

and hence that $\mu(p, \beta)$ is concave with respect to p ,

$$\mu \left(\frac{p+q}{2}, \beta \right) \leq \frac{1}{2} [\mu(p, \beta) + \mu(q, \beta)]. \quad (14)$$

(A slight modification of the standard argument shows that μ is also concave with respect to β). It is trivial that for $p \geq 1$,

$$Z_N(p) = \sum_G (Z_G)^p \leq \left(\sum_G Z_G \right)^p, \quad (15)$$

so that,

$$\mu(p, \beta) \leq p\mu(1, \beta), \quad p \geq 1. \quad (16)$$

We also have that,

$$\begin{aligned} \frac{\partial \mu(p, \beta)}{\partial p} &= \lim_{N \rightarrow \infty} \frac{1}{N} \frac{1}{Z_N} \frac{\partial}{\partial p} \left(\sum_G (Z_G)^p \right) \\ &= \lim_{N \rightarrow \infty} \frac{1}{Z_N} \sum_G (Z_G)^p \mu_G > 0 \end{aligned} \quad (17)$$

and hence that $\mu(p, \beta)$ is a concave monotonic increasing function with respect to p . However, μ is bounded by a linear function and hence it must be asymptotically linear in p as $p \rightarrow \infty$. Since the number of graphs with given Z_G does not depend upon p it must be the case that, as $p \rightarrow \infty$, $Z_N(p)$ is dominated by those graphs G_0 with largest Z_G so that,

$$\mu(p \rightarrow \infty) \sim p\mu_{G_0} \quad (18)$$

and it is therefore of some interest to identify these maximal graphs. This identification alone is not sufficient to solve the models at large p because the number of such graphs and fluctuations around them must be included to find the sub-asymptotic behaviour and, in particular, the value of γ_{str} .

In the following section we identify most of the maximal graphs for models I, II and III. For a given value of β we might suppose that there is a value $p_c(\beta)$ of p above which the maximal graphs dominate. (Of course it may be that the transition to dominance by maximal graphs is seamless and that there is no critical value or that $p_c(\beta) = \infty$ for all β .) In section 4 we begin to address the question of the behaviour of $p_c(\beta)$.

3.2 Model I

In this section we prove that the maximal graphs for model I are tree graphs with tadpoles at the ends of the branches (see fig 1 for an example).

Starting with an arbitrary N vertex ϕ^3 graph, select a point D and reconnect the links to it as shown in fig 2. The resulting graph still has N vertices, and provided that the link DC lay on a closed loop in the original graph, the new graph will still be connected. Repeat this procedure taking care not to disconnect the graph. Eventually there are no further links that can be cut and the graph is tree-like (ie there are no closed loops except for the tadpoles at the ends of the branches). Before the link DC is cut the partition function is

$$Z_1 = \frac{1}{2C^3} \sum_{S_a S_b S_c S_d} Z(S_a, S_b, S_c) \exp \beta(S_a S_d + S_b S_d + S_c S_d) \quad (19)$$

$$= \sum_{S_a S_b S_c} Z(S_a, S_b, S_c) (1 + t^2(S_a S_b + S_b S_c + S_c S_a)), \quad (20)$$

where $Z(S_a, S_b, S_c) (\geq 0)$ represents the partition function for the remainder of the graph with boundary spins S_a, S_b, S_c and $C = \cosh \beta$, $t = \tanh \beta$. After reconnecting the links, the new partition function is

$$Z_2 = \sum_{S_a S_b S_c} Z(S_a, S_b, S_c) (1 + t)(1 + t S_a S_b) \quad (21)$$

so that,

$$Z_2 - Z_1 = \sum_{S_a S_b S_c} Z(S_a, S_b, S_c) t(1 + S_a S_b)(1 - t S_b S_c) \geq 0. \quad (22)$$

Thus at each step the partition function increases (equality occurs for $\beta = 0$ and $\beta = \infty$). The partition function takes the same value,

$$Z_{tree} = (1 + \tanh \beta)^{\frac{N}{2}+1} \quad (23)$$

for all tree graphs with N vertices, so we have proved that the set of tree graphs is maximal for all finite non-zero β . This set of graphs does not magnetize at finite β . We will need later the number of tree

Figure 1: Tree-like graph

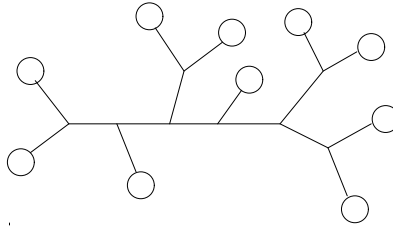
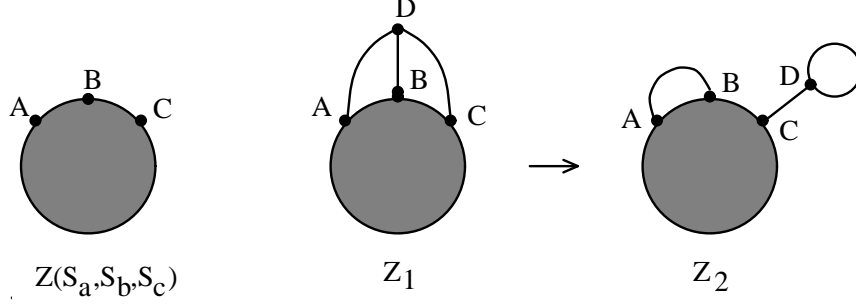


Figure 2: Partition functions



graphs with N vertices which is given by [27]

$$\mathcal{G}_{tree}(N) = \frac{(N-2)!}{(\frac{1}{2}N+1)!(\frac{1}{2}N-1)!} \underset{N \rightarrow \infty}{\sim} e^{N \log 2} N^{-\frac{5}{2}}. \quad (24)$$

In considering the contributions of different graphs to $Z_N(p)$ at finite p (which we will do in sections 5 and 6) it is useful to examine the ratio,

$$\frac{Z_2}{Z_1} = \left(1 - \frac{t}{(1+t)^2} \langle 1 + S_a S_b - t(S_b S_c + S_a S_c) \rangle_{G_2} \right)^{-1}, \quad (25)$$

where

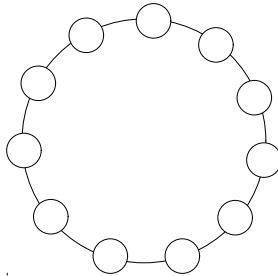
$$\langle Q \rangle_{G_2} \equiv \frac{1}{Z_2} \sum_{S_a S_b S_c} Z(S_a, S_b, S_c) (1+t)(1+t S_a S_b) Q. \quad (26)$$

For small t , $\langle S_a S_b \rangle = 1$ or is of order t (depending on whether or not A and B are distinct points), while $\langle S_b S_c \rangle$, $\langle S_a S_c \rangle \sim O(t^m)$ with $m \geq 1$; thus Z_2/Z_1 increases with t at small t so that tree-like graphs are becoming more important. Assuming that $p_c(\beta)$ is finite, it is decreasing with β in this region. On the other hand, for large enough t , $\langle S_a S_b \rangle$, $\langle S_b S_c \rangle$, $\langle S_a S_c \rangle \approx 1$ and Z_2/Z_1 decreases towards one as $t \rightarrow 1$, so that tree-like graphs become less important again. The position of any minimum of the curve $p_c(\beta)$ must lie between these two regimes.

3.3 Model II

For model II, the maximal graphs are ring graphs (fig 3) and again this is true for any value of β . The proof, which is very similar to that for model I, consists of two parts. Firstly, we show that any graph in this model can be converted into a ring graph by a series of steps, where none of the intermediate graphs contain tadpoles. Secondly, we show that the partition function increases at each step and thus that ring graphs are maximal for all β .

Figure 3: Ring graph



For ϕ^3 graphs of genus zero the number of faces, F , is related to the number of edges, E , through $F = 2 + \frac{1}{3}E$. Defining f_i to be the number of faces with i sides, then $F = \sum f_i$ and $E = \frac{1}{2} \sum i f_i$ so that,

$$\sum_i f_i \left(1 - \frac{i}{6}\right) = 2. \quad (27)$$

Since $f_i \geq 0$, in order for the equation to be satisfied we must have $f_i \neq 0$ for some $i < 6$. Thus, any ϕ^3 graph in this model must contain a 2-loop (ie a loop of length two), a triangle, a square or a pentagon.

Starting with a graph G , containing no tadpoles, replace any subgraphs such as that in figure 4a (which we will call dressed propagators) with bare propagators (fig 4b), yielding a new ϕ^3 graph, G' , to which the above theorem applies. Putting the dressed propagators back we recover G and have shown that it contains at least one of the following: a dressed 2-loop, or a dressed or bare triangle, square or pentagon. The only exception is the ring graph, which upon making the replacement shown in fig 4 just gives a circle for graph G' . Thus, any graph, except for the ring, contains one of the subgraphs in the above list.

Dressed propagators containing n 2-loops will be drawn as in fig 4c. We are going to replace the subgraphs fig 5a to fig 8a with subgraphs fig 5b to fig 8b respectively. The number of vertices is unchanged and the number of 2-loops is increased by these replacements. In appendix A we show that the partition function increases, for any choice of dressed propagators in the original subgraph (ie for all choices of $j, k, l, m, n \geq 0$; for the 2-loop case, fig 5a, n, m are not both zero). Thus by choosing the orientation of the replacement, we can create a new graph, which is connected, has no tadpoles, has the same number of vertices as the original and has a larger partition function. By repeatedly eliminating the subgraphs in the above list we will eventually end up with a ring graph, proving that the ring graphs are maximal for all β . The partition function for the ring graph is given by,

$$Z_{ring} = (1 + t^2)^{\frac{N}{2}} + (2t^2)^{\frac{N}{2}} \quad (28)$$

and this graph does not magnetize for any finite β .

Figure 4: (a) Dressed (b) Bare (c) Renormalized propagators

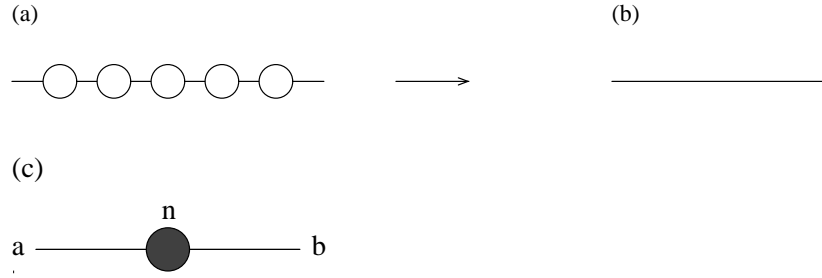


Figure 5: (a) 2-loop (b) Replacement subgraph or equivalently (c)

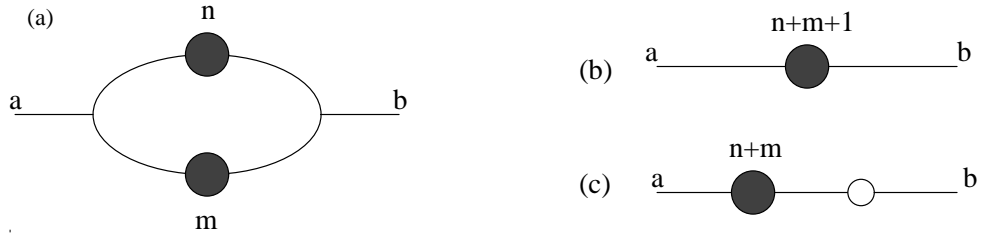


Figure 6: (a) Triangle (b) Replacement subgraph

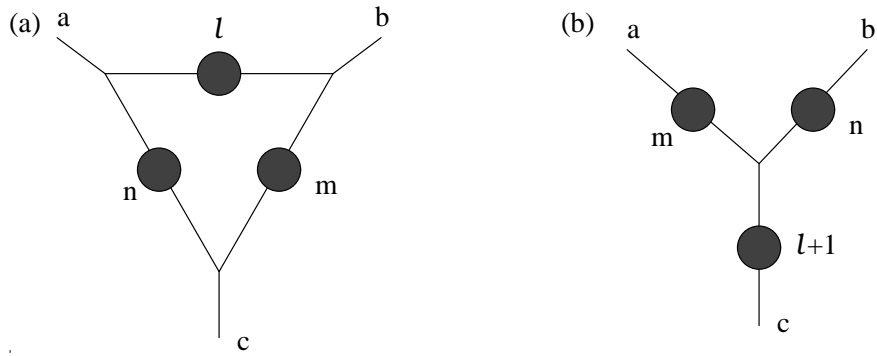


Figure 7: (a) Square (b) Replacement subgraph

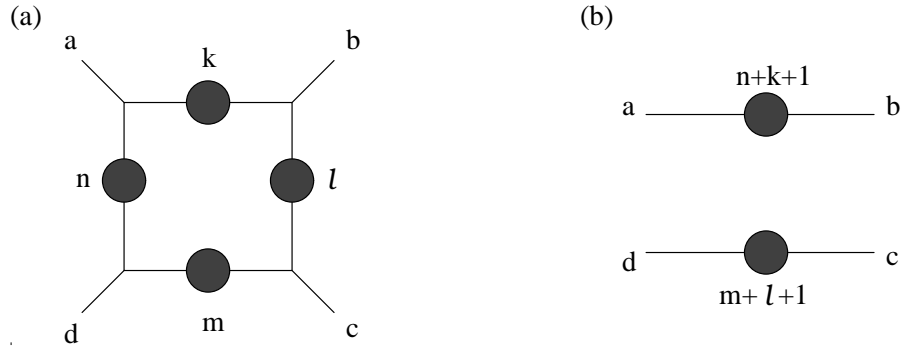
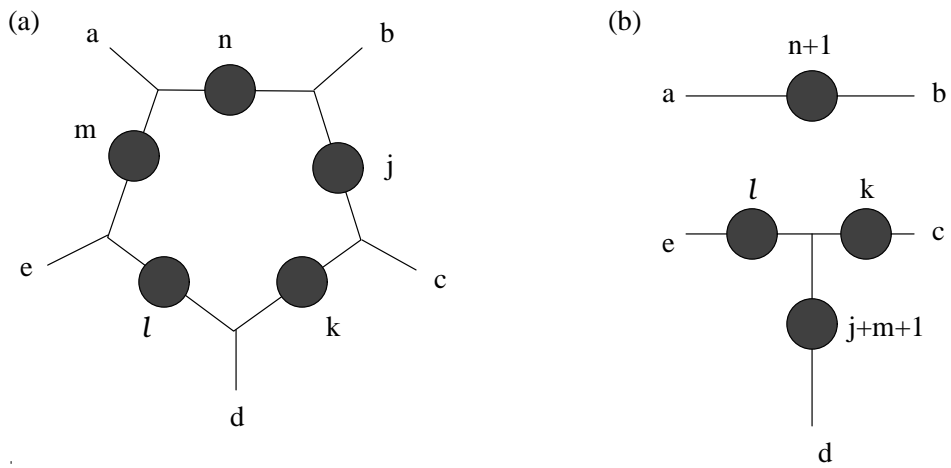


Figure 8: (a) Pentagon (b) Replacement subgraph



3.4 Model III

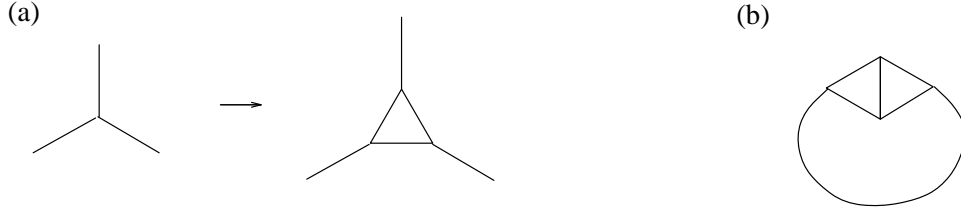
In this case we have not found a procedure which converts any given graph into a maximal graph; essentially this is because the form of the maximal graph now depends on β . We have identified the maximal graphs for the limits of small and large β , but not for intermediate values of β .

A high temperature expansion ($\beta \rightarrow 0$) of the partition function for a given graph gives,

$$Z_G = 1 + \sum_l n_l t^l, \quad (29)$$

where n_l is the number of closed, but possibly disconnected, non-self-intersecting loops in the graph that contain l links. For model III, $n_1 = n_2 = 0$ because we have eliminated tadpoles and self-energies and the first non-zero coefficient is n_3 , the number of triangular loops. The maximum possible value of n_3 is the integer part of $\frac{N}{3}$ which we will denote by $\lfloor \frac{N}{3} \rfloor$. Suppose that N is divisible by three, then taking any graph with $\frac{1}{3}N$ points and replacing each point with a triangle (fig 9a), gives an N vertex graph with $n_3 = \frac{N}{3}$. If N is not divisible by three, replace all except one or two of the points giving $n_3 = \lfloor \frac{N}{3} \rfloor$. To show that this really is the maximum possible number, first note that the only case which has two triangles back to back is the tetrahedron (fig 9b). Then, ignoring this case, given an N vertex graph we can collapse all of its triangular loops to points and get a graph with N' vertices and no tadpoles or self-energies. Clearly $N' \geq n_3$ (since each collapsed triangle yields a vertex) and $N' = N - 2n_3$ (as collapsing a triangle removes two vertices). Thus $N - 2n_3 \geq n_3$ and so $n_3 \leq \frac{N}{3}$. Hence the maximum value is $n_3 = \lfloor \frac{N}{3} \rfloor$ for $N > 4$.

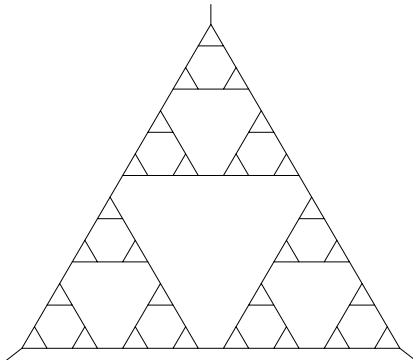
Figure 9: (a) Replacement (b) Tetrahedron



Consider graphs, G , for which the total number of points is $N = 2 \times 3^n$, where n is some sufficiently large integer. In order to maximize Z_G in the $\beta \rightarrow 0$ limit, we maximize each coefficient in turn. Having maximized n_3 as described above by replacing each point of G' (with $\frac{1}{3}N$ points) with a triangle we now choose G' in order to maximize the next coefficients. The replacement of points with triangles doubles the number of edges bordering each face of G' , which being a model III graph has a smallest loop length of three. Any such loops will be doubled to length six; thus $n_4 = n_5 = 0$. Now, $n_6 = n_6^c + \frac{1}{2}n_3(n_3 - 1)$ (where n_6^c is the number of connected loops of length six), so that we need to maximize n_6^c next. To do this we must maximize n_3 of G' (since loops of length three in G' become those of length six in G). So we take a graph with $\frac{1}{9}N$ points and make the replacement of points with triangles to get G' . Carrying on in this fashion we end up with a fractal graph (see fig 10). If $\frac{1}{2}N$ is not a power of three, then the graph will not quite be regular, but will still be essentially fractal-like.

At large β , graphs which magnetize can be studied in the low temperature expansion for which,

Figure 10: Fractal graph



$$Z_G = \frac{1}{Z_0} 2e^{\frac{3N}{2}\beta} \left(1 + \sum_{r=3}^{\infty} m_r x^r \right) \sim \frac{1}{Z_0} \exp N \left(\frac{3}{2}\beta + \sum_{s=3}^{\infty} a_s x^s \right), \quad (30)$$

where $x = e^{-2\beta}$ and m_r is the number of domain boundaries that cross r links. For graphs with no tadpoles or self-energies any domain boundary must cross at least three links so that the sum starts at $r = 3$ and the sum for the free energy also starts at $s = 3$. However, this does not apply to graphs that do not magnetize; the ladder graph (fig 11) has $m_3 \propto N$, but $m_4 = \frac{1}{2}N(\frac{N}{2} - 1)$ so we might expect it to exponentiate to give a series starting at $s = 2$ with $a_2 = \frac{1}{2}$. It is straightforward to check that this is the case from the ladder free energy, which is given by,

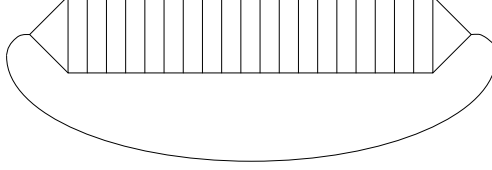
$$\mu_{ladder} = \frac{1}{2} \log \left(\frac{1}{2} \left(1 + t^2 + \sqrt{(1 - t^2)^2 + 4t^4} \right) \right). \quad (31)$$

Because these graphs are one-particle irreducible it is not possible to get $m_2 \propto N^2$ and a_1 is always zero. We conclude that at large β the ladder graphs, whose free energy starts at $O(x^2)$, will dominate magnetizable graphs, whose free energy starts at $O(x^3)$. Furthermore it is easy to check that μ_{ladder} is bigger than that of the fractal graph for large β .

What happens at intermediate β is not clear but is probably quite complicated, involving graphs which in some sense interpolate between the fractal and the ladder graphs; whether the transition from fractal to ladder is continuous or discontinuous we cannot say, but the former seems more likely on grounds of universality with models I and II - but maybe this system is not universal. Neither the fractal nor the ladder magnetize so probably the intermediate graphs do not magnetize either and as $p \rightarrow \infty$ the model only magnetizes at $\beta \rightarrow \infty$.

It is interesting to note that for a Gaussian model on a random triangulation embedded in D dimensions [27, 28, 29, 30, 31] the maximal graphs (for $D > 0$) are those with the minimal number of spanning trees and that the corresponding ϕ^3 graphs are tree graphs, ring graphs and ladders for models I to III respectively. Thus the maximal Ising graphs at large β are the same as the maximal graphs for the Gaussian model, but they apparently differ at small β in the case of model III. Reference [27] lists the maximal

Figure 11: Ladder graph



graphs, but gives a more symmetric version of the ladder graph; presumably that is because fig 11 is excluded from the relevant model even though it has no tadpoles or self-energies.

4 Truncated models

4.1 Model I

To get some indication of how large p must be before the maximal graphs become dominant we now consider a truncated model in the weak coupling regime. For small β ,

$$\mu_G = \frac{1}{N} \left[n_1 t + \left(n_2 - \frac{1}{2} n_1^2 \right) t^2 + \left(n_3 - n_1 n_2 + \frac{1}{3} n_1^3 \right) t^3 + \dots \right], \quad (32)$$

so we consider a model for which μ_G is truncated to

$$\mu_G^T = \frac{n_1}{N} t. \quad (33)$$

The grand canonical partition function for this model is then,

$$\mathcal{Z}(\mu, pt) = \sum_{\substack{N=2 \\ \text{even}}}^{\infty} e^{-\mu N} \sum_{n_1=0}^{\infty} \mathcal{G}^{(1)}(N, n_1) e^{n_1 pt}, \quad (34)$$

where $\mathcal{G}^{(1)}(N, n_1)$ is the number of graphs with N vertices and n_1 tadpoles (loops of length one) ($0 \leq n_1 \leq \frac{1}{2}N + 1$). We show in appendix B.2 that $\mathcal{G}^{(1)}(N, n_1)$ satisfies the recurrence relation,

$$\mathcal{G}^{(1)}(N+2, n_1+1) = \left(\frac{3N-2n_1}{n_1+1} \right) \mathcal{G}^{(1)}(N, n_1) + 2\mathcal{G}^{(1)}(N, n_1+1) \quad (35)$$

and the total number of graphs is known so

$$\sum_{n_1=0}^{\frac{1}{2}N+1} \mathcal{G}^{(1)}(N, n_1) = \mathcal{G}^{(1)}(N), \quad (36)$$

where $\mathcal{G}^{(1)}(N)$ is given in (7). Using the recurrence relation (35) and putting $y = e^{pt}$, $x = e^{-\mu}$ we find that \mathcal{Z} satisfies the differential equation,

$$\frac{\partial \mathcal{Z}}{\partial y}(1 + 2x^2(y - 1)) = 3x^3 \frac{\partial \mathcal{Z}}{\partial x} + x^2 y, \quad (37)$$

which has the solution,

$$\mathcal{Z} = \frac{1}{12x^2} \left(h^{\frac{3}{2}} - 1 \right) + \frac{1}{2}(y - 1) - \frac{1}{4} \log h + \sum_{\substack{N=2 \\ \text{even}}}^{\infty} \mathcal{G}^{(1)}(N) x^N h^{-\frac{3N}{4}}, \quad (38)$$

where $h = (1 - 4x^2(y - 1))$. The asymptotic behaviour at large N is thus given by

$$\mathcal{Z} \sim \sum_N \mathcal{G}^{(1)}(N) x^N h^{-\frac{3N}{4}} \sim \sum_N N^{-\frac{7}{2}} \exp -N \left(\mu + \frac{3}{4} \log h - \frac{1}{2} \log(12\sqrt{3}) \right), \quad (39)$$

so the thermodynamic free energy $\mu_c(pt)$ obeys the cubic equation,

$$\mu_c + \frac{3}{4} \log(1 - 4e^{-2\mu_c}(y - 1)) - \frac{1}{2} \log(12\sqrt{3}) = 0. \quad (40)$$

The solution is

$$\begin{aligned} \mu_c(pt) = \log 2 + \frac{1}{2} \log(y - 1) - \frac{1}{2} \log \left[1 - \frac{9}{(y - 1)^2} - 3 \left(\frac{1}{2(y - 1)^2} \right)^{\frac{1}{3}} \times \right. \\ \left. \sum_{\sigma=\pm 1} \omega^{\sigma} \left(1 - \frac{18}{(y - 1)^2} + \frac{54}{(y - 1)^4} + \sigma \sqrt{1 - \frac{4}{(y - 1)^2}} \right)^{\frac{1}{3}} \right], \end{aligned} \quad (41)$$

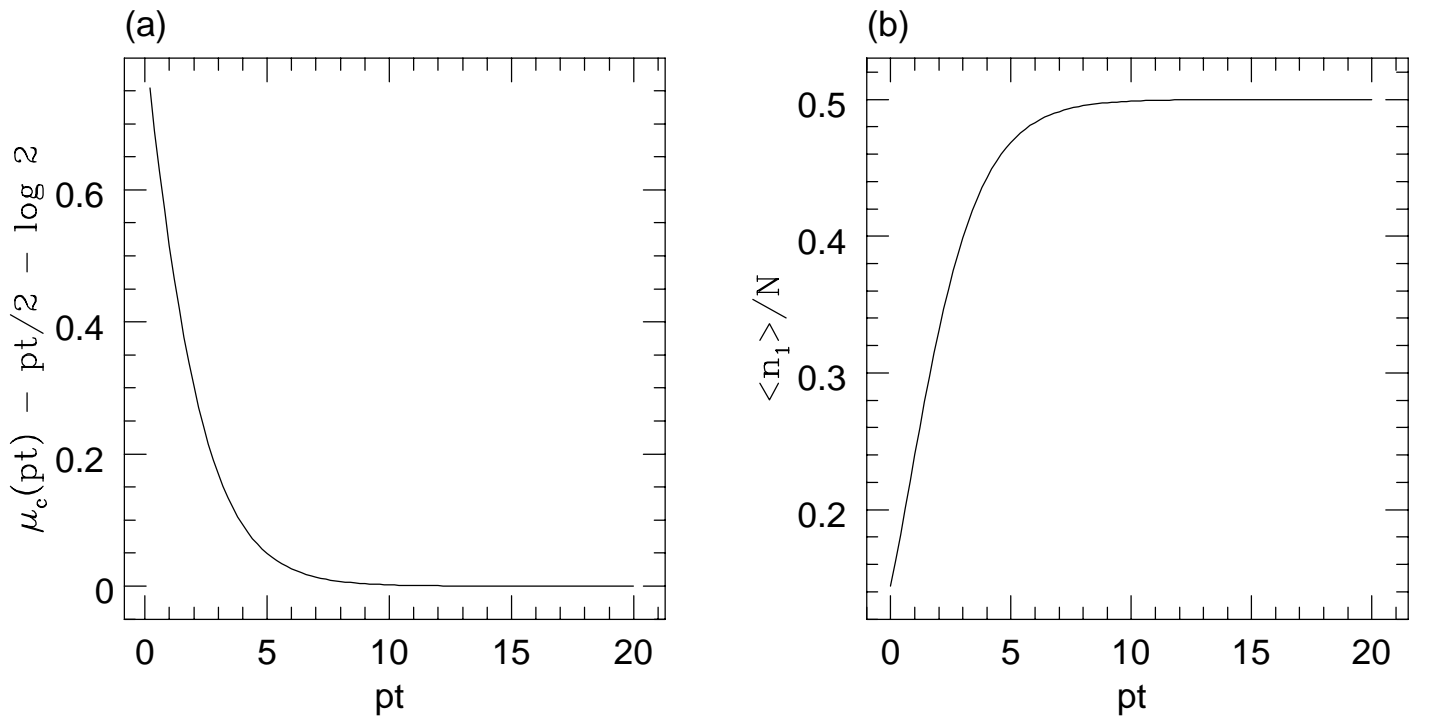
with $\omega = e^{\frac{2\pi i}{3}}$ for $y < 3$ and $\omega = 1$ for $y > 3$ (the solution and its derivatives are actually continuous across $y = 3$). The solution is plotted in fig 12a where it is compared to $\mu_c' = \frac{1}{2}pt + \log 2$, which is what we would expect if trees were totally dominant. We see that $\mu_c(pt)$ approaches μ_c' quite rapidly as pt increases, but it is necessary to have $p \rightarrow \infty$ for the trees to dominate completely. It is also interesting to examine the ratio $r \equiv \langle n_1 \rangle / N$, which is shown in fig 12b; for $pt > 6$ the ratio is very close to one half and the fact that the gradient changes very quickly near this point leads us to suspect that the full model might develop a discontinuity in one of its derivatives at some finite value of p (ie $p_c(\beta)$). A formula for r can be derived from that for \mathcal{Z} ; putting $b = 2e^{-pt}$, $\lambda = \frac{4b^2}{(3b-2)(b+2)}$,

$$r = \frac{1}{2-b} \left[1 + \lambda^{\frac{1}{3}} \left(\omega \left(1 - \sqrt{1-\lambda} \right)^{\frac{1}{3}} + \omega^2 \left(1 + \sqrt{1-\lambda} \right)^{\frac{1}{3}} \right) \right], \quad (42)$$

where ω is a cube root of unity and we need to use $\omega = 1$ for $0 \leq b < \frac{2}{3}$ and $\omega = e^{\frac{2\pi i}{3}}$ for $\frac{2}{3} < b \leq 2$ (the solution and derivatives are continuous across $b = \frac{2}{3}$).

As is shown by (39) the string susceptibility $\gamma_{str} = -\frac{1}{2}$ for all finite p in this truncated model; only for $p = \infty$ does γ_{str} change to $\frac{1}{2}$, but, again, in the full model this change may occur at some finite $p_c(\beta)$.

Figure 12: Truncated model (model I)



4.2 Model III

This calculation can be repeated for model III, which has,

$$\mu_G = \frac{1}{N}(n_3 t^3 + n_4 t^4 + n_5 t^5 + (n_6 - \frac{1}{2}n_3^2)t^6 + \dots). \quad (43)$$

We truncate μ_G to

$$\mu_G^T = \frac{n_3}{N} t^3 \quad (44)$$

where $0 \leq n_3 \leq \lfloor \frac{N}{3} \rfloor$. The grand canonical partition function is defined as

$$\mathcal{Z}(\mu, pt^3) = \sum_{\substack{N=6 \\ \text{even}}}^{\infty} e^{-\mu N} \sum_{n_3=0}^{\infty} \mathcal{G}^{(3)}(N, n_3) e^{n_3 p t^3}, \quad (45)$$

where $\mathcal{G}^{(3)}(N, n_3)$ is the number of graphs in model III with N vertices and n_3 loops of length three. This obeys a recurrence relation, derived in appendix B.1,

$$\mathcal{G}^{(3)}(N+2, n_3+1) = \left(\frac{N-3n_3}{n_3+1} \right) \mathcal{G}^{(3)}(N, n_3) + 3\mathcal{G}^{(3)}(N, n_3+1), \quad (46)$$

which holds for $N \geq 6$. The recurrence relation (46) gives, putting $y = e^{pt^3}$ and $x = e^{-\mu}$,

$$\frac{\partial \mathcal{Z}}{\partial y} (1 + 3x^2(y-1)) = x^3 \frac{\partial \mathcal{Z}}{\partial x} + \frac{1}{3} x^6 y. \quad (47)$$

The solution is

$$\mathcal{Z}(\mu, pt^3) = -\frac{1}{3} \left(hx - \frac{1}{2}x^2 + \frac{1}{4}x^4 \right) + \sum_{\substack{N=2 \\ \text{even}}}^{\infty} \mathcal{G}^{(3)}(N) h^N, \quad (48)$$

where $\mathcal{G}^{(3)}(N)$ is given by (9) and $h = x + x^3(y-1)$. Thus for large N ,

$$\mathcal{Z} \sim \sum_N \mathcal{G}^{(3)}(N) h^N \sim \sum_N N^{-\frac{7}{2}} \exp N \left(\frac{1}{2} \log \left(\frac{256}{27} \right) + \log(x + x^3(y-1)) \right). \quad (49)$$

Solving for $\mu_c(pt^3)$ as in the previous case gives

$$\mu_c(pt^3) = -\frac{1}{2} \log 3 + \frac{5}{3} \log 2 + \frac{1}{3} \log(y-1) - \log \left[\sum_{\sigma=\pm 1} \left(1 + \sigma \sqrt{1 + \left(\frac{32}{27} \right)^2 \frac{1}{y-1}} \right)^{\frac{1}{3}} \right]. \quad (50)$$

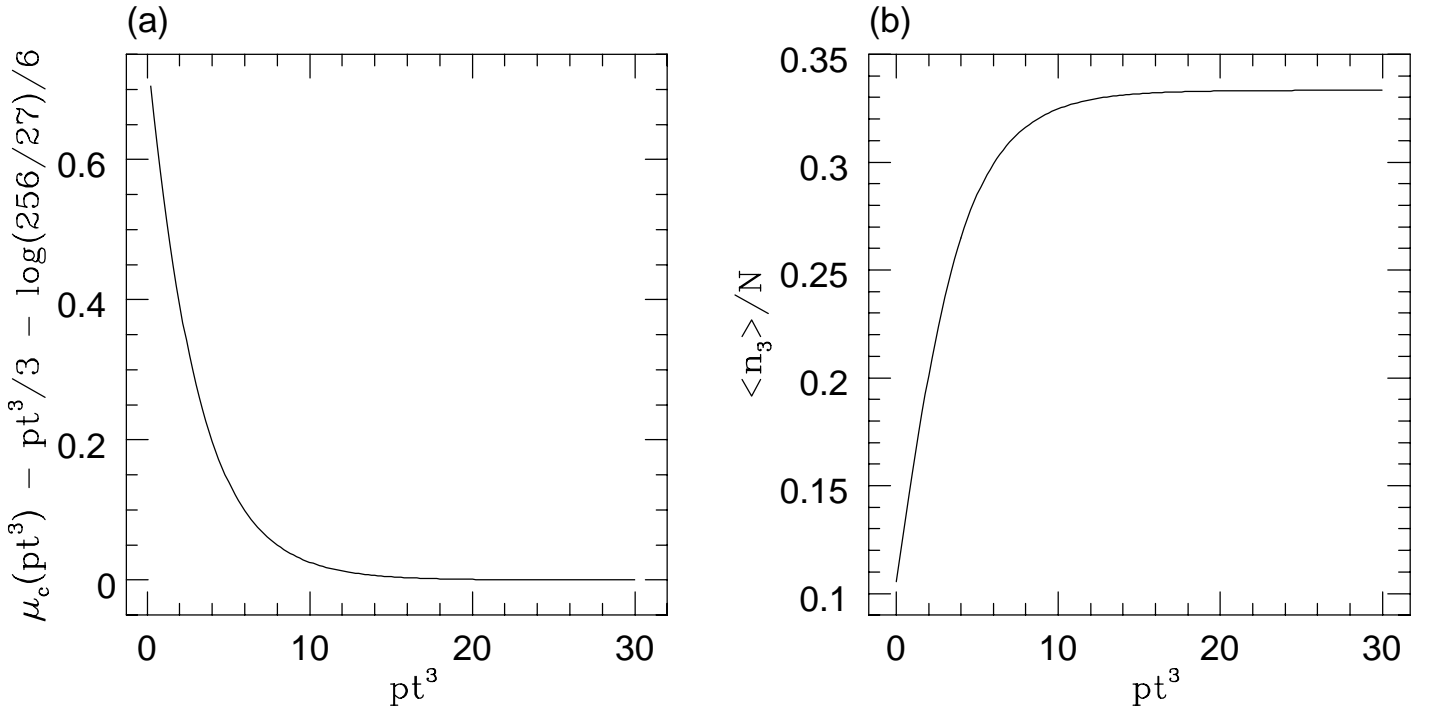
We can also calculate $\langle n_3 \rangle / N$,

$$\frac{\langle n_3 \rangle}{N} = \frac{1}{a} \left[1 - \left(\frac{1}{2} \left(\frac{3-a}{12-ca} \right) \right)^{\frac{1}{3}} \sum_{\sigma=\pm 1} \left(1 + \sigma \sqrt{1 - 4 \left(\frac{3-a}{12-ca} \right)} \right)^{\frac{1}{3}} \right], \quad (51)$$

where $a = 3(1 - e^{-pt^3})$ and $c = 295/256$. Again, this saturates as p is increased (see fig 13b).

Looking at the graph (fig 13a) of $\mu_c(pt^3) - \frac{1}{3}pt^3 - \frac{1}{6}\log\left(\frac{256}{27}\right)$ (where the last term takes account of the exponential number of graphs with $\frac{n_3}{N} = \frac{1}{3}$) we see that for $pt^3 > 8$ the behaviour is essentially linear, because after this point the integral is being dominated by a single type of graph (ie those graphs with $n_3 \approx \frac{1}{3}N$). However, it should be noted that in this truncated model we again need $p = \infty$ in order to actually reach $n_3/N = \frac{1}{3}$ and the set of such graphs is quite large (not just fractal-like graphs). This is due to the fact that μ_G has been truncated to the first term (n_3), but higher order terms are needed to show that fractals are maximal for $\beta \rightarrow 0$. Again, $\gamma_{str} = -\frac{1}{2}$ for all finite values of p .

Figure 13: Truncated model (model III)



5 Magnetization transition

5.1 Derivation of a bound on β_c

In this section we derive a bound on the critical value of the coupling constant, β_c , for the case of a single Ising spin ($p = 1$) on a fixed graph G . This implies a bound on the critical coupling for magnetization related phase transitions in models I, II and III. The high temperature expansion of Z_G (29) gives,

$$Z_G = 1 + \sum_l n_l t^l = \exp \left(\sum_{l=1}^{\infty} a_l t^l \right). \quad (52)$$

Now consider,

$$Z_{G'} = \exp \left(\sum_{l=1}^{\infty} n_l^c t^l \right), \quad (53)$$

where n_l^c is the number of connected, non-backtracking closed loops of length l . Expanding the exponential yields all closed non-intersecting loops, but in addition it gives loops in which some links are used more than once so that $Z_G < Z_{G'}$ and therefore

$$\mu_G < \frac{1}{N} \sum_{l=1}^{\infty} n_l^c t^l. \quad (54)$$

However the number of non-backtracking closed loops of length l originating at a given point is less than 2^l so

$$\mu_G < \sum_{l=1}^{\infty} (2t)^l. \quad (55)$$

Thus the high temperature series for μ_G must converge if $t < \frac{1}{2}$; it follows that any phase transition on G must occur at a $t_c \geq \frac{1}{2}$ (ie $\beta_c \geq 0.549$).

A slight modification of this argument excludes the possibility of permanently magnetized graphs. Fix one spin S_+ to be +1, so the magnetization $M_G(\beta)$ is given by,

$$M_G(\beta) = \frac{1}{N} \sum_+ \frac{1}{N} \frac{1}{Z_G} \frac{1}{2^{N-1}} \sum_{\{S\}} \sum_i S_i \prod_{\langle a,b \rangle} (1 + t S_a S_b), \quad (56)$$

where the \sum_+ runs over all possible locations of the fixed spin (this is necessary because unlike the regular lattice model any two given spins may be almost disconnected from one another). The only contribution to the numerator comes from paths connecting S_i to S_+ , so

$$M_G(\beta) = \frac{1}{N^2} \frac{\sum_+ 2^{N-1} \sum_i \sum_l d_l(i, +) t^l}{\sum_{\{S\}} \prod_{\langle a,b \rangle} (1 + t S_a S_b)}, \quad (57)$$

where $d_l(i, +)$ is the number of paths of length l from S_i to S_+ (which can be disconnected, but are non-self-intersecting and non-backtracking). However,

$$\sum_l d_l(i, +) t^l = \sum_l w_l(i, +) t^l (1 + b_1 t + b_2 t^2 + \dots), \quad (58)$$

where $w_l(i, +)$ is the number of connected paths of length l from S_i to S_+ and the b_l series gives the contributions from the closed loops, which do not intercept the path. The denominator, however, contains contributions from all closed loops and hence is larger than $2^{N-1} \sum_l b_l t^l$ so

$$M_G(\beta) < \frac{1}{N^2} \sum_+ \sum_i \sum_l w_l(i, +) t^l. \quad (59)$$

However, $\sum_i w_l(i, +)$ is just the number of connected paths of length l from S_+ and we know that this is less than 2^l . Thus,

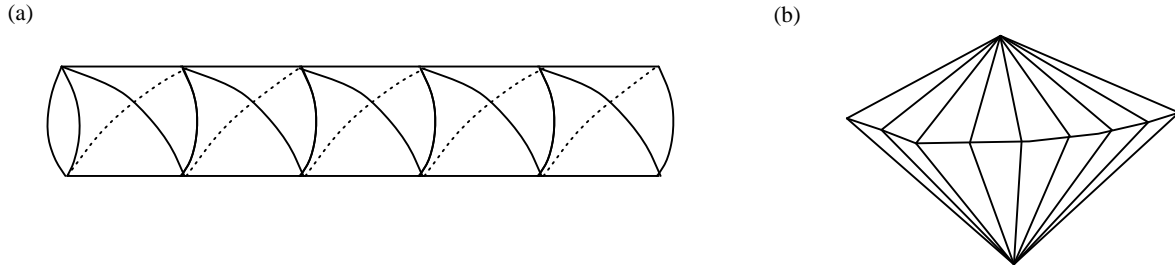
$$M_G(\beta) < \frac{1}{N} \sum_l (2t)^l = \frac{1}{N} \frac{1}{1-2t}, \quad (60)$$

for $t < \frac{1}{2}$ and hence $M_G(\beta) \rightarrow 0$ as $N \rightarrow \infty$. If more than one spin is fixed to be $+1$, then the right hand side of this equation is multiplied by the number of such spins, so that to avoid $M_G(\beta) \rightarrow 0$ a number of spins proportional to N must be fixed. That is, we need to fix a thermodynamically significant number of spins in order to get the system to magnetize and thus there can be no spontaneously magnetized state for $t < \frac{1}{2}$.

This result was derived for a single graph, but obviously still applies when we perform a summation over graphs; no phenomena associated with magnetization can occur at $t < \frac{1}{2}$.

For the ϕ^3 graphs the high temperature ($\beta \rightarrow 0$) expansion converges for $\tanh \beta < \frac{1}{2}$, this implies that on the dual triangulation the low temperature ($\beta \rightarrow \infty$) expansion converges for $e^{-2\beta} < \frac{1}{2}$ (ie for $\beta > \frac{1}{2} \log 2 \approx 0.347$). Thus any critical value of β must satisfy $\beta_c \leq \frac{1}{2} \log 2$, on the triangulated surface. In contrast with ϕ^3 graphs, there exist both graphs which never magnetize and those which are permanently magnetized (see fig 14). The argument showing that there are no permanently magnetized ϕ^3 graphs, can not be used for the dual triangulation because the relation $\sum_i w_l(i, +) < 2^l$ no longer holds. This is due to the fact that the vertices can have coordination numbers greater than three (in fact the permanently magnetized graph shown has points with coordination numbers of order N).

Figure 14: Triangulations: (a) never magnetizes; (b) permanently magnetized



5.2 Mechanisms of magnetization

For this model the magnetization can be written as

$$M(p, \beta) = \frac{\sum_G \frac{1}{s_G} M_G(Z_G)^p}{\sum_G \frac{1}{s_G} (Z_G)^p}, \quad (61)$$

where $M_G(\beta)$ is the magnetization for a given N -vertex graph G , and we are taking the limit $N \rightarrow \infty$. In the limit $p \rightarrow 0$ we effectively have a quenched magnetization,

$$M_0(\beta) \equiv M(0, \beta) = \frac{1}{\mathcal{G}(N)} \sum_G \frac{1}{s_G} M_G(\beta), \quad (62)$$

where $\mathcal{G}(N)$ is the number of graphs with N vertices in whichever model is being looking at. This case has recently been investigated numerically [32]. The critical value for the magnetization of this model will be denoted by β_c and the critical coupling constant for a given graph G by β_G^* . One can show that the behaviour of $M_0(\beta)$ at β_c only depends on those graphs which magnetize near β_c . We will illustrate this by proving the result for the case in which graphs G undergo a first order phase transition; in this case only those graphs for which $\beta_c - \epsilon < \beta_G^* \leq \beta_c$, (where ϵ is an arbitrary small positive number) contribute to $M_0(\beta_c)$. In actual fact the phase transitions of individual graphs are second order, however the extension of the result to this case is relatively straightforward and is omitted. Now,

$$M_0(\beta) = \frac{1}{\mathcal{G}(N)} \left[\sum_{G: \beta_G^* \leq \beta - \epsilon} M_G(\beta) + \sum_{G: \beta_G^* > \beta - \epsilon} M_G(\beta) \right], \quad (63)$$

where the notation $G: \beta_G^* \leq \beta - \epsilon$ means that we are summing over graphs G for which the inequality is satisfied and we have absorbed the symmetry factors into the summations. Since the system magnetizes at β_c ,

$$M_0(\beta_c - \epsilon) = \frac{1}{\mathcal{G}(N)} \sum_{G: \beta_G^* \leq \beta_c - \epsilon} M_G(\beta_c - \epsilon) \xrightarrow{N \rightarrow \infty} 0. \quad (64)$$

For a first order transition in which each graph jumps to M_G^0 at its critical point,

$$\frac{1}{\mathcal{G}(N)} \sum_{G: \beta_G^* \leq \beta_c - \epsilon} M_G(\beta_c - \epsilon) \geq \frac{1}{\mathcal{G}(N)} \sum_{G: \beta_G^* \leq \beta_c - \epsilon} M_G^0 \geq \min(M_G^0) \frac{1}{\mathcal{G}(N)} \sum_{G: \beta_G^* \leq \beta_c - \epsilon} 1. \quad (65)$$

While,

$$\frac{1}{\mathcal{G}(N)} \sum_{G: \beta_G^* \leq \beta_c - \epsilon} M_G(\beta_c) \leq \frac{1}{\mathcal{G}(N)} \sum_{G: \beta_G^* \leq \beta_c - \epsilon} 1 \leq \frac{1}{\min(M_G^0)} \frac{1}{\mathcal{G}(N)} \sum_{G: \beta_G^* \leq \beta_c - \epsilon} M_G(\beta_c - \epsilon), \quad (66)$$

which tends to zero by (64). Hence (63) gives

$$M_0(\beta_c) = \frac{1}{\mathcal{G}(N)} \sum_{G: \beta_G^* > \beta_c - \epsilon} M_G(\beta_c) = \frac{1}{\mathcal{G}(N)} \sum_{G: \beta_c - \epsilon < \beta_G^* \leq \beta_c} M_G(\beta_c), \quad (67)$$

so that only graphs which magnetize near β_c contribute to $M_0(\beta_c)$. As it stands the proof cannot be used for second order transitions (where $M_G^0 = 0$), but careful consideration shows that in this case only graphs for which $\beta_c - \epsilon < \beta_G^* \leq \beta_c + \delta$ (where ϵ, δ are small positive numbers) can contribute to $M_0(\beta_c + \delta)$. Thus the critical exponents can only depend on the behaviour of graphs which are magnetizing near the critical point β_c and the magnetization is as a result of spin-ordering of these graphs.

For non-zero p , a different geometric type of transition is possible and this seems to be what occurs for large p . In this case the magnetization is caused by the changing of the relative weights between different graphs. This can best be understood by looking at a simple model in which there are only two types of graph; suppose that there are n_1 unmagnetized graphs ($n_1 \sim \exp f_1 N$) with partition function $Z_1 \sim \exp \mu_1 N$ and n_2 magnetizable graphs ($n_2 \sim \exp f_2 N$) with magnetization $m(\beta)$ and partition function $Z_2 \sim \exp \mu_2 N$. Then assuming that the magnetizable graphs are the more numerous ($f_2 > f_1$) and have smaller partition functions ($\mu_2 < \mu_1$), which is certainly the case if we are looking at transitions to tree graphs in model I, the partition function is

$$Z_N(p) = n_1 Z_1^p + n_2 Z_2^p \underset{N \rightarrow \infty}{\sim} e^{(f_1 + p\mu_1)N} + e^{(f_2 + p\mu_2)N} \quad (68)$$

and the magnetization,

$$M(p, \beta) \underset{N \rightarrow \infty}{\sim} \frac{1}{Z_N(p)} m(\beta) e^{(f_2 + p\mu_2)N}. \quad (69)$$

In the thermodynamic limit the magnetization $M(p, \beta)$ is zero if $f_1 + p\mu_1 > f_2 + p\mu_2$, that is, if $p(\mu_1 - \mu_2) > (f_2 - f_1)$. As β is varied the difference $\mu_1 - \mu_2$ changes and at the point for which the inequality no longer holds (β_c) the magnetization jumps from zero to $m(\beta_c)$. Thus there is a first order transition.

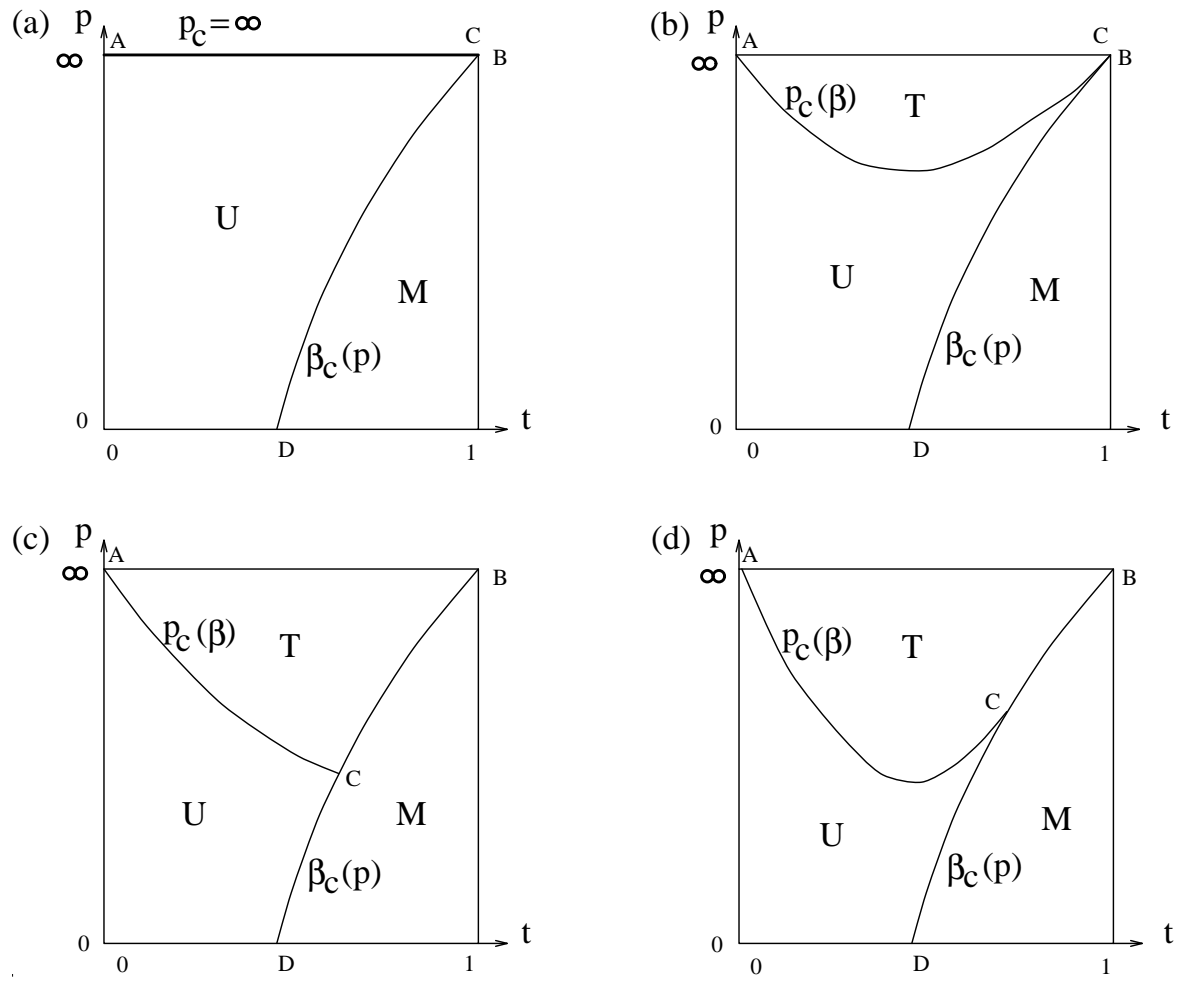
In the large p limit for which $\beta_c \rightarrow \infty$ it is possible in model I to have magnetized graphs with $r \equiv n_1/N$ arbitrarily close to $\frac{1}{2}$, so that even if the transition is generically first order the discontinuity, Δr , could be zero in this limit (ie perhaps $\Delta r \rightarrow 0$ as $p \rightarrow \infty$). For $p \rightarrow \infty$ there is such a transition, for model I, between unmagnetized tree graphs and magnetized non-tree-like graphs, with no discontinuity [15, 16].

6 Conclusion

In figure 15 we have drawn possible forms of the phase diagram for model I. The magnetized region is labelled M, the tree-like region T and the remaining unmagnetized non-tree-like region U. We would expect similar diagrams for models II and III, but in the latter case it is not clear what is happening in the T region, as we have not identified the maximal graphs for intermediate values of β .

For models I and II, we know that the partition functions of graphs increase as we replace closed loops with disconnected structures. Since the graphs are becoming less well-connected one might expect that they tend to magnetize at higher values of β and have lower magnetizations at a given value of β . As p is increased in this model, the graphs with the larger partition functions make a relatively larger contribution to $Z_N(p)$ and so we expect that $\beta_c(p)$ will increase. There is some evidence for this from numerical simulations [19, 20, 21, 23]. We might also expect the magnetization, for a fixed β , to decrease as p is increased and again there is some evidence for this from Monte Carlo simulations [20]. It should of course be noted that these simulations were for model III, for which we do not know the maximal graphs. However, since all the maximal graphs that we *have* identified are not well-connected and do not

Figure 15: Possible phase diagrams



magnetize, it is quite likely that this also applies for model III at intermediate values of β ; it also follows that in none of the models do we expect $\beta_c(p \rightarrow \infty)$ to be finite.

In the papers of Wexler [15, 16] the $p \rightarrow \infty$ limit of model I is studied in the low temperature (large β) expansion. In this limit there is a critical coupling $e^{-2\beta_c} \sim 1/p$ below which the dominant graphs are tree-like being made up of large numbers of almost disconnected baby universes within which the spins are all aligned. This phase has $\gamma_{str} = \frac{1}{2}$ and our results indicate that this behaviour must persist beyond the large β expansion, in fact for all $\beta > 0$. Above β_c the dominant graphs contain few baby universes each of whose volume (number of vertices) is very large and $\gamma_{str} = -\frac{1}{2}$; thus it seems that the properties of the M region do not depend strongly on p . At the critical point, where both the number of baby universes and their volume diverge, it is found that $\gamma_{str} = \frac{1}{3}$. This result is also found in the paper of Ambjørn et al [17] who considered a restricted model in which only phase interfaces of minimum length are allowed; they obtain the result that the exponent at the critical point γ^* is related to that in the large β phase, $\bar{\gamma}$, by $\gamma^* = \bar{\gamma}/(\bar{\gamma} - 1)$ so long as $\bar{\gamma} < 0$. This phase transition at $p \rightarrow \infty$ is geometrical, as discussed in section 5.2, rather than one of spin alignment; it occurs because the partition functions of magnetized graphs are catching up with the others. It seems highly likely that this phenomenon will persist to finite p although a calculation of the $1/p$ corrections (or equivalently the contribution of domain boundaries of length greater than two in the model of [17]) is needed to rule out the phase diagram of 15b analytically.

The extent of the tree-region T is not yet fully understood. We know that at $\beta = 0$, where the Ising partition function is one, the model is independent of p and has $\gamma_{str} = -\frac{1}{2}$; in addition, the absence of extra transitions in models with $c < 1$ suggests that the line AC separating the U and T regions does not go below $p = 2$. We cannot rule out the possibility that $p_c(\beta) = \infty$ as shown in figure 15a. However, the truncated models do display a region of relatively rapid changeover to the T region and it seems likely that the full models have a phase transition (with $p_c t \approx 6$, $p_c t^3 \approx 8$ for models I and III respectively at small enough t).

For model I, $x \equiv \frac{1}{2} - r$ (where $r = n_1/N$ is the ratio of loops of length one to vertices) serves as an order parameter. In the region T, $x = 0$ and approaching the line AC from below at fixed β , we would expect x to decrease continuously to zero, that is a second (or higher) order phase transition. This is because, just below the critical line, the largest contributions to $Z_N(p)$ come from diagrams which are tree-like except for a number of closed loops. As p is increased the number of closed loops (excluding loops of length one) decreases to zero in a continuous fashion (see for example fig 12b, which shows how $\langle r \rangle$ approaches a half as p is varied, for the truncated model).

The transition to T from M across CB is rather different. Then we know that just below the critical line the partition function is dominated by magnetized graphs (which cannot be tree-like or almost tree-like, as such graphs do not magnetize for $t \neq 1$) and such graphs have $r \neq \frac{1}{2}$. Thus we might expect there to be a first order transition with r jumping discontinuously. It is tempting to hypothesise that for the line DC between the M and U regions there is a continuous spin-ordering transition whose characteristics are determined by the graphs which are actually magnetizing at the critical point $\beta_c(p)$, as happens for the quenched case ($p \rightarrow 0$). On the other hand the line CB between the T and M regions is a geometrical phase transition in which the transition is caused by the changes in geometry due to the changing relative weights (ie Z_G^p) of the magnetized and tree-like graphs.

For model III, there is direct numerical evidence from computer simulations. In this case it is not as clear what we should use as an order parameter for the U T transition, but n_5/N (the ratio of closed loops of length five to vertices) seems a plausible candidate. For both the fractal and ladder graphs this quantity is zero and if, as seems possible, the intermediate maximal graphs consist of mixtures of fractals

arranged in a ladder-like fashion, then it would be zero in the whole T region. Unfortunately, none of the numerical studies looked at this quantity in detail. Reference [20] measure the quantity for $p = 16$ (in fig 12 of that paper), but only at the critical point β_c , where it is very close to its pure gravity value. However, references [18, 19, 20] do give graphs of n_3/N for various values of β . This quantity peaks at some value of β below β_c and drops to the pure gravity value as $\beta \rightarrow 0$ or $\beta \rightarrow \beta_c$. The height of the peak grows with p in an apparently linear fashion, but we know that it is bounded by the relation $n_3/N \leq \frac{1}{3}$. It would be interesting to see how this quantity saturates as p is increased, for β near β_c , and to compare it with the results we have from the truncated model in the limit of small β .

It is interesting to examine the average maximal radius, r_{max} , of the ensemble. For a given graph r_{max} is defined in the following fashion. Take an arbitrary point on the graph (called the “centre”), mark all of its neighbours as being at a distance one from the centre, mark all the unmarked neighbours of these points as being at distance two and so on. The maximal extension is then the distance of the furthest point from the centre and averaging over different centres gives r_{max} on the graph. This procedure can be carried out on either the ϕ^3 graph or the dual triangulation, giving two different definitions, which we will denote r_{max}^G and r_{max}^T respectively. In figure 7 of [20] r_{max}^T is plotted for various different models; the curve has a minimum for values of β just below β_c and its depth increases with p up to the maximum value considered, $p = 16$. Both fractals and ladders have very small values of r_{max}^T and so as the T phase is approached one would expect r_{max}^T to fall. Let p^* be the value of p at the point C in fig 15c and now suppose that p is held fixed at $p < p^*$ and we approach the magnetization transition from the U region; then as β increases we also get closer to the T region and thus might expect to see a decrease in r_{max}^T , which disappears when the system magnetizes. As $p \uparrow p^*$ this effect would become more pronounced until at p just above p^* we expect to see a sharp transition into a branched polymer-like phase which immediately disappears as β increases and the system magnetizes; r_{max}^T would decrease sharply as the critical region around C is approached and then rebound when the system magnetizes. This behaviour seems very like that observed in [20] which suggests to us that even the largest value of p used in the simulation is probably no greater than p^* . If p is significantly greater than p^* we would expect the minimum value of r_{max}^T , when the ensemble is most branched polymer-like, to occur somewhere in the middle of the T region rather than at the magnetization transition; so as p increases beyond p^* the minimum of r_{max}^T will move away from the magnetization transition. It is difficult to be entirely certain in interpreting the behaviour of r_{max}^T without knowing how the minimum value scales with N ; it would be useful to have simulation data on this and also at much larger p to be certain of our interpretation.

Although we have worked entirely with Ising models many of our considerations probably extend to other spin systems which have second order phase transitions on regular lattices; in particular the maximal graphs and the general behaviour of the truncated models are likely to be the same.

We would like to thank Thórdur Jónsson for giving us advanced details of [17] and to acknowledge the support of the SERC under grant GR/J21354 and through the research studentship GR/H01243.

A Proof that ring graphs are maximal

In order to complete the proof that rings are maximal for model II, we need to show that each of the subgraphs listed in section 3.3 can be eliminated in a way that increases the partition function.

Consider the case for the 2-loop first. A propagator dressed with n 2-loops and joining spins S_a to S_b (fig 4c), has a contribution of

$$G^{(n)}(S_a, S_b) = 2^{2n} C^{3n+1} ((1+t^2)^n + S_a S_b t^{2n+1} 2^n) = C'(1+t' S_a S_b), \quad (70)$$

where $C = \cosh \beta$, $t = \tanh \beta$ and

$$C' = 2^{2n} C^{3n+1} (1+t^2)^n \quad (71)$$

$$t' = \left(\frac{2t^2}{1+t^2} \right)^n t \equiv Y^n t. \quad (72)$$

Thus dressing a propagator effectively renormalizes the coupling constant for that link. The partition function for the whole of the original graph is given by

$$\sum_{S_a S_b} Z(S_a, S_b) Z_1(S_a, S_b), \quad (73)$$

where $Z(S_a, S_b)$ is the partition function of the remainder of the graph ($Z(S_a, S_b) \geq 0$) and Z_1 is that for the subgraph being replaced (fig 5a). The partition function for the graph after the replacement has Z_1 replaced by Z_2 (fig 5c). The powers of two and the factors of C and C' are the same for both graphs and cancel with terms in Z_0^{-1} , so that we can drop these factors which gives,

$$Z_1 = 1 + Y^{n+m} t^2 + S_a S_b t^3 (Y^n + Y^m), \quad (74)$$

$$Z_2 = 1 + t^2 + S_a S_b (2t^3 Y^{n+m}). \quad (75)$$

Hence,

$$\Delta Z = t^2 (1 - Y^{n+m} + S_a S_b t (2Y^{n+m} - Y^n - Y^m)) \quad (76)$$

$$= t^2 ((1 - Y^n) (1 - S_a S_b t Y^m) + Y^n (1 - Y^m) (1 - S_a S_b t)) \geq 0. \quad (77)$$

Noting that $0 \leq Y, t \leq 1$ and $n, m \geq 0$, we can see that ΔZ is not negative and that $\Delta Z = 0$ occurs for $t = 0$ and $t = 1$, as we would expect. The partition function of the graph is increased by the replacement in fig 5.

The triangular case (fig 6) can be proven in the same way as the 2-loop case. However, for the square and pentagon, the expression for ΔZ is so complicated that it is extremely difficult to regroup the terms and write ΔZ in a form which is manifestly non-negative. An inductive method can be used to prove each of the cases and we will indicate below how one would use it to prove the case of the square (fig 7). For this case we need to prove that $\Delta Z_{klmn}(S_a, S_b, S_c, S_d)$ where

$$\begin{aligned} \Delta Z_{klmn} t^{-2} &= 2+t (S_a S_b Y^k (2Y^n - 1) + S_c S_d Y^m (2Y^l - 1) - S_b S_c Y^l - S_d S_a Y^n) + \\ &\quad t^2 (1 - Y^{k+l+m+n} - S_a S_c (Y^{k+l} + Y^{n+m}) - S_b S_d (Y^{m+l} + Y^{n+k})) + \\ &\quad t^3 (S_a S_b Y^n (2Y^k - Y^{l+m}) + S_c S_d Y^l (2Y^m - Y^{n+k}) - S_b S_c Y^{k+n+m} - S_d S_a Y^{m+l+k}) + \\ &\quad t^4 S_a S_b S_c S_d (4Y^{k+l+m+n} - Y^{k+m} - Y^{n+l}), \end{aligned} \quad (78)$$

is positive for all $0 < t < 1$, and all values of the spins, S_a, S_b, S_c, S_d . It is easy to prove that $\Delta Z_{0000} > 0$ for $0 < t < 1$ and any values of the spins S_a, S_b, S_c, S_d . We define a difference operator D_k by

$$D_k \Delta Z_{klmn} = \Delta Z_{(k+1)lmn} - Y \Delta Z_{klmn} \quad (79)$$

and similarly for D_l, D_m, D_n . Now, ΔZ_{klmn} has the form,

$$\Delta Z_{klmn} = A + Y^k B, \quad (80)$$

where A, B are independent of k , but in general depend on all the other variables. Hence,

$$D_k \Delta Z_{klmn} = (1 - Y)A, \quad (81)$$

which is independent of k ; note that $(1 - Y)$ is a positive factor. Now,

$$\Delta Z_{(k+1)lmn} = Y \Delta Z_{klmn} + D_k \Delta Z_{klmn}. \quad (82)$$

If we can show that $D_k \Delta Z_{klmn} > 0$ for any l, m, n and similarly for D_l, D_m and D_n acting on ΔZ , then, since $\Delta Z_{0000} > 0$, the result $\Delta Z_{klmn} > 0$ for all $k, l, m, n \geq 0$ follows by induction.

In order to prove that $D_k \Delta Z_{klmn} > 0$ we use the fact that the difference operators commute so that,

$$D_k \Delta Z_{kl(m+1)n} = Y(D_k \Delta Z_{klmn}) + D_m(D_k \Delta Z_{klmn}). \quad (83)$$

Now we need to prove that $D_k \Delta Z_{k000} > 0$ and that $D_m D_k \Delta Z_{klmn} > 0$ (and similarly for all pairs of difference operators). Proceeding in this way the problem is reduced to showing that the following quantities are positive: ΔZ_{0000} , $D_k \Delta Z_{k000}$ (similarly for D_l etc), $D_k D_l \Delta Z_{kl00}$ (similarly for all possible pairs), $D_k D_l D_m \Delta Z_{klm0}$ (all possible triples) and $D_k D_l D_m D_n \Delta Z_{klmn}$. Each of these expressions depends only on t and the spins, and is thus relatively easy to prove (especially if a computer is used to check each case). Thus finally we have $\Delta Z_{klmn} > 0$ for $0 < t < 1$. The pentagonal case can be proved in the same fashion.

B Derivation of recurrence relations

B.1 Model III

The recurrence relation (46) for two-particle irreducible planar graphs is derived by considering the effect of replacing a point P, on a graph G , by a triangle. Such a replacement increases the number of vertices in the graph by two and increases the number of triangular loops (n_3) by either one (fig 9a) or zero (fig 16) depending on whether or not the point P of graph G was lying on a triangle. Note that since self-energy terms have been eliminated the only possible diagram for which P could lie on two triangles is given by fig 9b, which has $N = 4$ vertices; we shall ignore this case and derive a recurrence relation valid for $N \geq 6$.

Graphs with $N + 2$ vertices and $n_3 + 1$ triangles can be made from those with N vertices and n_3 triangles by replacing one of $N - 3n_3$ points (fig 9a), or from graphs with N vertices and $n_3 + 1$ triangles by replacing one of $3(n_3 + 1)$ points (fig 16). We will refer to the points which yield the correct number of triangles when replaced (ie $n_3 + 1$) as being ‘allowed’ points. Clearly all such graphs can be made by this method.

We need to determine the effect of such a replacement on the symmetry factor of a graph. Suppose that graph G has symmetry group \mathcal{G} of order s . Since G is planar we can think of it as being a polyhedron and the members of \mathcal{G} as being rotations. By making rotations we can interchange a point P with any of a set R (of size f_1) of equivalent points. Now, rotations that leave P in the same position give a subgroup \mathcal{H} of \mathcal{G} which has order s/f_1 (which will equal either one or three, since there are three lines emerging from each vertex). Replacing P by a triangle T , we group the triangles of the new graph G' into equivalence classes. If T is a member of a class of size f_2 then the order of the symmetry group of G' is $s' = sf_2/f_1$.

If we consider the equivalence classes of all the allowed points in all graphs with N vertices, then there is a one-to-one correspondence between these classes and the classes of triangles in all the graphs with $N+2$ vertices. A replacement of a point P by a triangle T defines a mapping between classes of points and of triangles. Let us associate a weight $f_1/s = f_2/s'$ for this mapping between classes. That is, we are associating a weight of $1/s$ for each allowed point in a graph that is being mapped from, or equivalently a weight of $1/s'$ for each triangle in a graph that is being mapped to. The total weight for allowed points is given by,

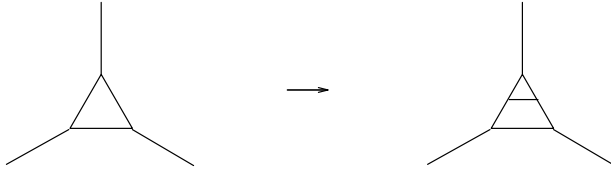
$$\begin{aligned} \sum_{\text{graph } i} \sum_{\text{allowed points}} \frac{1}{s_i} &= \sum_{\substack{\text{graph } i \\ (N, n_3)}} (N - 3n_3) \frac{1}{s_i} + \sum_{\substack{\text{graph } j \\ (N, n_3+1)}} 3(n_3 + 1) \frac{1}{s_j} \\ &= (N - 3n_3) \mathcal{G}^{(3)}(N, n_3) + 3(n_3 + 1) \mathcal{G}^{(3)}(N, n_3 + 1). \end{aligned} \quad (84)$$

However, this is equal to the weight for the graphs being mapped to, due to the one-to-one correspondence, which is

$$\sum_{\substack{\text{graph } i \\ (N+2, n_3+1)}} \sum_{\text{triangles}} \frac{1}{s'_i} = \sum_{\text{graph } i} (n_3 + 1) \frac{1}{s'_i} = (n_3 + 1) \mathcal{G}^{(3)}(N + 2, n_3 + 1). \quad (85)$$

Equating these gives the claimed result.

Figure 16: Replacement does not change n_3

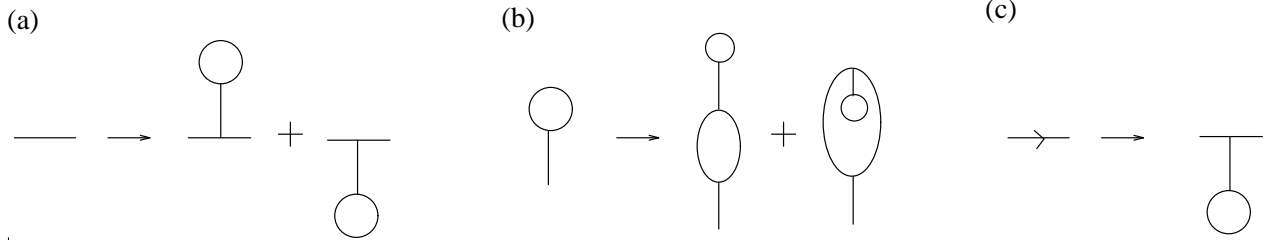


B.2 Model I

The recurrence relation (35) for model I can be derived in a similar fashion, by considering the addition of a tadpole to a link (see fig 17a). There is the added complication that the tadpole can be orientated in one of two different directions, (we distinguish between these configurations because they are counted separately in the matrix model). We will consider the creation of graphs with $N + 2$ vertices and $n_1 + 1$

tadpoles, from N point graphs with either n_1 tadpoles (see fig 17a) or $n_1 + 1$ tadpoles (fig 17b). For the $N + 2$ vertex graphs we will group the tadpoles into equivalence classes. However, there are no rotations that leave a given tadpole fixed (since this would correspond to rotating a polyhedron, whilst keeping an edge and an adjacent face fixed, which is impossible). Thus, rotations just interchange the tadpoles within each equivalence class in a cyclic fashion and the order of the symmetry group, s' , is just equal to the size of the equivalence classes (all of them being the same size). (Incidentally, this means that the order of the symmetry group of a graph divides the number of tadpoles. Hence, if the number of tadpoles is prime, p , then the graph has a symmetry factor of either 1 or $1/p$.)

Figure 17: (a) Replacement (b) Replacement on tadpole (c) Orientated version



For the N point graphs, we decompose the graphs into sets of allowed links (that is, links which when we add a tadpole to them give us a total of $n_1 + 1$ tadpoles). Each N point graph has $\frac{3N}{2}$ links and $3N$ orientated links (ie we count each link twice; once with an arrow going in one direction and once with the arrow reversed). The orientated links are collected into classes which contain links that can be rotated into each other. A link may or may not be in the same class as its reversed version. It is impossible to make a rotation that leaves a link in the same position and with the same orientation. As a result, we again have that the equivalence classes are all of the same size, which is equal to the order of the symmetry group, s . Now, the addition to an orientated link (as in fig 17c) of a tadpole on the right-hand side, defines a mapping between equivalence classes of allowed links in N point graphs and of tadpoles in $N + 2$ vertex graphs. This mapping is again one-to-one. The sizes of the equivalence classes equal the orders of the symmetry groups, so that the number of classes for a graph equals the number of allowed links divided by the order of the group. Equating the numbers of equivalence classes, we get,

$$\sum_{\substack{\text{graph } i \\ (N, n_1)}} 2 \left(\frac{3N}{2} - n_1 \right) \frac{1}{s_i} + \sum_{\substack{\text{graph } j \\ (N, n_1 + 1)}} 2(n_1 + 1) \frac{1}{s_j} = \sum_{\substack{\text{graph } k \\ (N + 2, n_1 + 1)}} (n_1 + 1) \frac{1}{s_k} \quad (86)$$

$$2 \left(\frac{3N}{2} - n_1 \right) \mathcal{G}^{(1)}(N, n_1) + 2(n_1 + 1) \mathcal{G}^{(1)}(N, n_1 + 1) = (n_1 + 1) \mathcal{G}^{(1)}(N + 2, n_1 + 1), \quad (87)$$

which gives the claimed result.

References

- [1] V.G.Knizhnik, A.M.Polyakov and A.B. Zamolodchikov, Mod. Phys. Lett. A3 (1988) 819
- [2] F.David, Mod. Phys. Lett. A3 (1988) 1651
- [3] J.Distler and H.Kawai, Nucl. Phys. B321 (1989) 509
- [4] E.Brézin and V.A.Kazakov, Phys. Lett. B236 (1990) 144
- [5] D.J.Gross and A.A.Migdal, Phys. Rev. Lett. 64 (1990) 127
- [6] M.R.Douglas and S.H.Shenker, Nucl. Phys. B335 (1990) 635
- [7] E.Brézin and S.Hikami, Phys. Lett. B283 (1992) 203
- [8] S.Hikami and E.Brézin, Phys. Lett. B295 (1992) 209
- [9] S.Hikami, Phys. Lett. B305 (1993) 327
- [10] M.L.Mehta, Commun. Math. Phys. 79 (1981) 327
- [11] V.A.Kazakov, Phys. Lett. A119 (1986) 140
- [12] V.A.Kazakov, Nucl. Phys. B (Proc. Suppl.) 4 (1988) 93
- [13] D.V.Boulatov and V.A.Kazakov, Phys. Lett. B186 (1987) 379
- [14] Z.Burda and J.Jurkiewicz, Acta Phys. Pol. B120 (1989) 949
- [15] M.Wexler, Nucl. Phys. B410 (1993) 377
- [16] M.Wexler, Mod. Phys. Lett. A8 (1993) 2703
- [17] J.Ambjørn, B.Durhuus and T.Jónsson, Preprint NBI-HE-94-02 (1994)
- [18] C.F.Baillie and D.A.Johnston, Mod. Phys. Lett. A7 (1992) 1519
- [19] C.F.Baillie and D.A.Johnston, Phys. Lett. B286 (1992) 44
- [20] J.Ambjørn, B.Durhuus, T.Jónsson, G. Thorleifsson, Nucl. Phys. B398 (1993) 568
- [21] M.Bowick, M.Falcioni, G.Harris and E.Marinari, Preprint SU-HEP-93-4241-556 and hep-th/9310136 (1993)
- [22] J.Ambjørn and G.Thorleifsson, Phys. Lett. B323 (1994) 7
- [23] J.-P.Kownacki and A.Krzywicki, Preprint LP THE Orsay 94/11 (1994)
- [24] E.Brézin, C.Itzykson, G.Parisi and J.B.Zuber, Commun. Math. Phys. 59 (1978) 35

- [25] W.T.Tutte, Can. J. Math. 14 (1962) 21
- [26] J.Koplik, A.Neveu and S.Nussinov, Nucl. Phys. B123 (1977) 109
- [27] D.V.Boulatov, V.A.Kazakov, I.K.Kostov and A.A.Migdal, Nucl. Phys. B275 [FS17] (1986) 641
- [28] V.A.Kazakov, I.K.Kostov and A.A.Migdal, Phys. Lett. B157 (1985) 295
- [29] J.Ambjørn, D.Durhuus, J.Fröhlich and P.Orland, Nucl. Phys. B270 [FS16] (1986) 457
- [30] F.David, Nucl. Phys. B257 [FS14] (1985) 543
- [31] J.Ambjørn, D.Durhuus and J.Fröhlich, Nucl. Phys. B257 [FS14] (1985) 433
- [32] C.F.Baillie, K.A.Hawick, D.A.Johnston, Preprint COLO-HEP-334, to be published in Phys. Lett. B